



Characterizing dynamic cerebral vascular reactivity using a hybrid system combining time-resolved near-infrared and diffuse correlation spectroscopy

DANIEL MILEJ,^{1,2,*}  MARWAN SHAHID,^{1,2} ANDROU ABDALMALAK,^{1,2} AJAY RAJARAM,^{1,2} MAMADOU DIOP,^{1,2}  AND KEITH ST. LAWRENCE^{1,2} 

¹Imaging Program, Lawson Health Research Institute, London, Ontario, N6A 4V2, Canada

²Department of Medical Biophysics, Western University, London, Ontario, N6A 5C1, Canada

*dmilej@laswonimaging.ca

Abstract: This study presents the characterization of dynamic cerebrovascular reactivity (CVR) in healthy adults by a hybrid optical system combining time-resolved (TR) near-infrared spectroscopy (NIRS) and diffuse correlation spectroscopy (DCS). Blood flow and oxygenation (oxy- and deoxy-hemoglobin) responses to a step hypercapnic challenge were recorded to characterize dynamic and static components of CVR. Data were acquired at short and long source-detector separations (r_{SD}) to assess the impact of scalp hemodynamics, and moment analysis applied to the TR-NIRS to further enhance the sensitivity to the brain. Comparing blood flow and oxygenation responses acquired at short and long r_{SD} demonstrated that scalp contamination distorted the CVR time courses, particularly for oxyhemoglobin. This effect was significantly diminished by the greater depth sensitivity of TR NIRS and less evident in the DCS data due to the higher blood flow in the brain compared to the scalp. The reactivity speed was similar for blood flow and oxygenation in the healthy brain. Given the ease-of-use, portability, and non-invasiveness of this hybrid approach, it is well suited to investigate if the temporal relationship between CBF and oxygenation is altered by factors such as age and cerebrovascular disease.

© 2020 Optical Society of America under the terms of the [OSA Open Access Publishing Agreement](#)

1. Introduction

Supporting the high energy demands of the brain requires continuous adjustments to vascular resistance to ensure adequate delivery of energy substrates by cerebral blood flow (CBF). The importance of CBF regulation to brain function, and conversely the link between cerebrovascular dysfunction and cognitive decline, has led to multiple approaches to assess cerebrovascular function involving different imaging techniques combined with various stimuli to elicit cerebral hemodynamic responses [1]. Because of carbon dioxide's potent vasodilatory effects, one of the most well-established markers of cerebrovascular function is cerebrovascular reactivity (CVR), which is defined as the ratio of the change in CBF in response to a change in arterial carbon dioxide pressure (PaCO_2).

The most commonly used methods of assessing CVR are magnetic resonance imaging (MRI), using blood-oxygenation level-dependent (BOLD) contrast as a surrogate of CBF, and transcranial Doppler, which measures blood flow velocity changes in a major cerebral artery. Both methods have been used to characterize changes in CVR related to ageing, head injuries, neurodegeneration, and cerebrovascular disease [2–5]. While BOLD MRI has the advantage of producing images of CVR, TCD is less expensive and portable, enabling more frequent assessments, evaluations in various environments (e.g., during surgery, part of neurocritical care, and in laboratory settings),

and simultaneous monitoring of systemic physiology not achievable in an MRI scanner. However, TCD does not assess cerebral microcirculation directly and must rely on assuming changes in flow velocities in a feeding artery reflect downstream perfusion changes and that the cross-sectional area of the insonicated vessel remains constant, which has been recently questioned [6].

Optical technologies – near-infrared spectroscopy (NIRS) and its flow-sensitive derivative, diffuse correlation spectroscopy (DCS) – share the same advantages as TCD in terms of portability, ease of use, and non-invasiveness, but have the added advantage of being sensitive to tissue hemodynamics. However, results with NIRS CVR studies have been mixed, with concerns regarding unexpected delays in the oxygenation responses relative to corresponding changes in blood flow velocity or BOLD contrast, inconsistent CVR measurements across subjects, and poor sensitivity [7–13]. The most likely explanation for these findings is signal contamination from extracerebral tissues considering these studies were conducted using continuous-wave NIRS devices, which are well known to be prone to extracerebral contamination. There have only been a couple of studies using DCS to measure CBF response to hypercapnia in adults [14,15]. Although both studies involved small sample sizes, DCS appears to provide more reliable CVR measurements across participants compared to NIRS, in-line with the predicted greater sensitivity of DCS to brain [9].

Another advantage of these optical techniques is their sub-second temporal resolution, which could be used to measure dynamic properties of CVR [16]. Recent BOLD studies have shown that the speed of the cerebrovascular response provides an additional and valuable metric of cerebrovascular function [17,18]. The combination of NIRS and DCS can extend this dynamic approach to enable simultaneous measurements of multiple hemodynamic parameters from the same brain region: CBF by DCS and oxy- and deoxy-hemoglobin concentrations by NIRS (HbO and Hb, respectively). The sum of HbO and Hb (i.e. tHb) is directly proportional to the cerebral blood volume (CBV) and the ratio of HbO to tHb defines tissue oxygen saturation (StO₂).

The aims of this study focused on evaluating if a hybrid system capable of acquiring NIRS and DCS data *simultaneously* could capture the dynamic CBF and oxygenation responses to a rapid step increase in end-tidal carbon dioxide pressure (P_{ET}CO₂). To minimize the effects of the CO₂ profile on the cerebral hemodynamic responses, a computer-controlled breathing circuit was used to generate abrupt changes in P_{ET}CO₂ [19]. The measured CBF and oxygenation responses were characterized using a hemodynamic response model proposed for BOLD CVR studies [17]. Given the evidence that NIRS CVR measurements are prone to extracerebral signal contamination [9,12], time-resolved detection (TR) was used to enhance depth sensitivity [20]. TR NIRS has been used to improve detection sensitivity of brain activity and to acquire accurate CBF estimates by bolus-tracking measurements [21,22]. Based on these previous findings, this study investigated if depth-enhanced oxygenation measurements would have greater reproducibility and better agreement with the hemodynamic model. Similarly, DCS data were acquired at two source-detector separations to vary the sensitivity to scalp and brain blood flow. These two time-courses were compared to the corresponding depth-enhanced oxygenation time course to investigate the sensitivity of DCS to CBF.

2. Methods

Eleven healthy participants (3 females, 8 males, aged 25 to 36 y, mean = 28 ± 3 y) with no history of any neurological or psychiatric disorders were recruited. Written informed consent was obtained from each subject prior to the experiment. The study was approved by the Western University Health Sciences Research Ethics Board, which adheres to the guidelines of the Tri-Council Policy Statement for research involving humans.

2.1. Experimental protocol

Subjects sat in a reclining chair with a gas mask placed over their mouth and nose. The mask was sealed by transparent film dressing (Tegaderm, 3M, St. Paul, USA) and connected to a computer-controlled gas delivery circuit (RespirAct™, Thornhill Research Inc, Toronto, Canada) [19]. A non-invasive monitoring system was secured to the participant's left arm (Finapres Medical Systems, Netherlands) to record heart rate (HR) and arterial blood pressure continuously (sampling rate = 200 Hz) during the experiment. A custom-designed probe holder was placed on the forehead and secured by a velcro headband. The holder was designed using SpaceClaim (ANSYS Inc., Canonsburg, USA), and 3D printed (TAZ 5, LulzBot, Loveland, USA) from a thermoplastic polyurethane material (Sapphire NinjaFlex, NinjaTek, Manheim, USA). Detection fibers for both subsystems were placed at a short and long source-detector separation (r_{SD}): 1.0 and 3.0 cm for TR NIRS, and 1.0 and 2.7 cm for DCS.

The experimental protocol consisted of three 2-min periods of hypercapnia. The first period started after two minutes at normocapnia, and each was followed by five minutes of normocapnia. The hypercapnia $P_{ET}CO_2$ target was set to 15 mmHg above each subject's normocapnic $P_{ET}CO_2$ value, which was defined by the automated gas controller. TR-NIRS and DCS data were acquired continuously throughout the cyclical $P_{ET}CO_2$ protocol at a sampling rate of 3.33 Hz.

2.2. TR-NIRS/DCS system

The TR-NIRS system consisted of two picosecond pulsed diode lasers (LDH-P-C, PicoQuant, Berlin, Germany) emitting at wavelengths (λ) of 760 and 830 nm, repetition rate of 80 MHz, and output powers less than 2.0 mW [23,24]. Custom made laser-to-fiber couplers (HPUC, OZ Optics, Ottawa, Canada) were used to couple light pulses from each laser head into a bifurcated fiber (NA = 0.39, ϕ = 400 μ m; Thorlabs, United States) [25] that guided the light to the skin surface. Diffusely reflected photons were collected by one fiber at a distance of 1 cm from the source (NA = 0.55, ϕ = 400 μ m; Fiberoptics Technology) and a fiber bundle at a distance of 3 cm (ϕ = 3 mm, NA = 0.22, length = 4 m, FiberTech Optica, Kitchener, Canada) [26]. Each delivered light to a hybrid photomultiplier detector (PMA Hybrid, PicoQuant, Berlin, Germany). To minimize signal contamination from the DCS laser, a short-pass interference filter was placed between collimating lenses in front of each detector (Spec 3551, 836.5 nm, ϕ = 25 mm, Alluxa, Santa Rosa, USA). The output of each detector was sent to a time-correlated single-photon counting module (HydraHarp 400, PicoQuant, Berlin, Germany) that generated the distribution of times-of-flight (DTOF) of photons.

At the end of every study, the instrument response function (IRF) was measured using a custom-built light-tight box that connected the emission fiber to a detection probe with a separation of 6 cm. A piece of white paper was placed in the light-path to disperse the light before it entered the detection probe. If necessary, a neutral density filter was placed in the box to avoid saturating the detector [27].

The DCS system used a continuous-wave laser emitting at λ = 850 nm with a coherence length greater than 10 m and emission power of 60 mW (DL852-100-SO; Crystalaser Inc., Reno, USA). The laser was coupled to a multimode fiber to deliver the light to the skin (NA = 0.22, ϕ = 400 μ m; Fiberoptics technology, Pomfret, USA). This fiber was separated by 1.2 cm from the TR-NIRS emission fiber to minimize signal contamination. Reflected light was collected by four single-mode fibers (SMF-28e+, NA = 0.14, ϕ = 8.2 μ m, single-mode cutoff λ = 1260 nm, FiberTech Optica, Kitchener, Canada), one at distance of 1 cm from the emission fiber and the remaining three at a distance of 2.7 cm. The latter fibers were bundled together with the fiber bundle for TR NIRS to provide a common detection point for the longer r_{SD} (i.e. 2.7 cm for DCS and 3 cm for TR NIRS).

Each DCS detection fiber was coupled to the input of a single photon counting module (SPCM-AQ4C; Excelitas Canada Inc., Toronto, Canada). Due to the large difference in power

between the DCS lasers and TR-NIRS lasers, filters in front of the DCS detectors were not required to block light from the TR-NIRS lasers. The output of each SPCM was relayed to a counter/timer data acquisition board (PCIE6612; National Instrument, Austin, USA). Photon counts were recorded and processed using in-house developed software (LabVIEW, National Instrument and MATLAB) to generate normalized intensity autocorrelation curves for 50 correlation times ranging from 1 μ s to 1 ms [28].

2.3. Crosstalk evaluation

In a subset of participants ($N = 4$), a series of tests were conducted to evaluate the magnitude of crosstalk between the two optical systems. With the probe holder placed on the forehead, data were collected from each system with and without light emission from the other source. The protocol consisted of three 1-min acquisitions: TR-NIRS acquisition, TR NIRS and DCS collected simultaneously, and DCS acquisition. The sequence was repeated three times with the same sampling rate and laser powers used in the hypercapnia experiments.

2.4. Data analysis

2.4.1. Systemic physiology

Steady-state baseline values of HR and mean arterial pressure (MAP) were obtained by averaging data acquired over a one-minute period immediately preceding each of the three hypercapnic period. Average HR and MAP responses to increased $P_{ET}CO_2$ were determined from the second minute of each hypercapnic period in order to allow the variables to reach a steady state. These time series were smoothed with a 4.5 s moving average with a zero-phase digital filter (filtfilt, MATLAB, Mathworks Inc., USA).

2.4.2. TR-NIRS analysis

To determine baseline optical properties at each r_{SD} , DTOFs recorded during two minutes of normocapnia prior to the first hypercapnic challenge were averaged. The mean DTOF was fit with the solution to the diffusion equation for a semi-infinite homogeneous medium convolved with the measured IRF (fminsearch, MATLAB, Mathworks Inc., USA). The fitting parameters were the absorption coefficient (μ_a), the reduced scattering coefficient (μ_s'), and an amplitude factor that accounts for laser power, detection gain, and coupling efficiency. The fitting range was set to 80% of the peak value of a DTOF on the leading edge and 20% on the falling edge [29].

Moment analysis was applied to each series of DTOFs as a means of extracting time courses of HbO and Hb concentration with varying depth sensitivities [30]. The first three statistical moments were calculated: total number of photons (N), mean time of flight ($\langle t \rangle$) and variance (V). Due to the positive skewness of the DTOF, $\langle t \rangle$ and V have been shown to be more sensitive to late-arriving photons [31]. The three moments were calculated for each recorded DTOF by setting the lower and upper integration limits to the arrival times corresponding to 3% (rise and fall) of the peak of the DTOF [30]. The change in each moment relative to its initial value was calculated to generate time series throughout the hypercapnia protocol (i.e., ΔN , $\Delta \langle t \rangle$ and ΔV) for $\lambda = 760$ and 830 nm individually.

To calculate changes in the concentrations of oxyhemoglobin and deoxyhemoglobin (ΔC_{HbO} and ΔC_{Hb} , respectively), each moment time series was converted to the corresponding change in $\Delta \mu_a(\lambda)$:

$$\Delta \mu_a(\lambda) = \frac{\Delta m_i}{SF_i}, \quad (1)$$

where Δm_i is the change in the i^{th} moment and SF_i is the corresponding sensitivity factor. The values of SF_i for N , $\langle t \rangle$ and V were determined using the solution to the diffusion approximation

for a semi-infinite homogeneous medium [22,32]. The final step was to convert $\Delta\mu(\lambda)$ determined at 760 and 830 nm into ΔC_{HbO} and ΔC_{Hb} using:

$$\Delta\mu_a(\lambda) = \varepsilon_{HbO}(\lambda)\Delta C_{HbO} + \varepsilon_{Hb}(\lambda)\Delta C_{Hb}, \quad (2)$$

where, $\varepsilon_{HbO}(\lambda)$ and $\varepsilon_{Hb}(\lambda)$ are the wavelength-dependent molar extinction coefficients for oxy- and deoxyhemoglobin, respectively.

This analysis resulted in time courses of ΔC_{HbO} and ΔC_{Hb} generated for each of the three moments individually. The sum of ΔC_{HbO} and ΔC_{Hb} were used to determine changes in the total hemoglobin concentration (ΔC_{tHb}), which reflects changes in CBV (ΔCBV), assuming no change in hemoglobin concentration. Changes in tissue oxygenation saturation (ΔStO_2) were determined from the standard definition of saturation: $StO_2 = C_{HbO} / (C_{HbO} + C_{Hb})$. Finally, least-squares optimization was used to regress a brain signal from the ΔC_{HbO} and ΔC_{Hb} time courses generated from ΔN for the two source-detector separations [33].

All time courses were smoothed with a 4.5-s moving average with a zero-phase digital filter (filtfilt, MATLAB, Mathworks Inc., USA).

2.4.3. DCS analysis

The autocorrelation curves acquired at the short and long distances were analyzed separately using the solution to the correlation diffusion equation for a semi-infinite homogenous medium. The fitting variables were the coherence factor (β), which relates the measured intensity autocorrelation function to the electric field autocorrelation function, and a blood flow index (BF_i). The latter is based on modelling perfusion as a pseudo Brownian motion [34], and BF_i values derived from this model have been shown to accurately track changes in CBF [35]. The baseline μ_a and μ_s' values determined at 830 nm by TR NIRS were used in the fitting routine. The fitting was performed across all correlation times from 1 μ s to 1 ms. The resulting BF_i time courses were smoothed with the same filter as the TR-NIRS data.

2.5. Cerebrovascular reactivity

The three hypercapnic periods were averaged to produce a single 7-min time course per subject for ΔC_{HbO} , ΔC_{Hb} , and BF_i . The procedure involved calculating the signal change relative to the baseline period prior to each hypercapnic challenge. These time courses were modelled as the convolution of the recorded step change in $P_{ET}CO_2$, $\Delta P_{ET}CO_2(t)$, which was scaled to a maximum value of one, and a hemodynamic response function (HRF) [17]:

$$\Delta S(t) = ssCVR \cdot [\Delta P_{ET}CO_2(t) * HRF(t)], \quad (3)$$

where, $\Delta S(t)$ is the signal change, ssCVR is the steady-state value of CVR and * denotes the convolution operator. The HRF is given by:

$$HRF(t) = \frac{1}{N} e^{-\frac{(t-t_o)}{\tau}}, \quad (4)$$

where, τ is the time constant defining the dynamic component of CVR, t_o is the time delay between the initial rise of $\Delta P_{ET}CO_2(t)$ and that of $\Delta S(t)$, and N is the area under $\int_0^\infty e^{-t/\tau} dt$. Best-fit estimates of τ , t_o and ssCVR were obtained by numerical optimization (fminsearchbnd, MATLAB, Mathworks Inc., USA). The fitting was performed over a time window that encompassed the hypercapnia period (i.e. from the initial rise in $\Delta P_{ET}CO_2(t)$ to end of the decline in $\Delta S(t)$ following the return of $P_{ET}CO_2$ to normocapnia). In some cases, the fitting range was only defined by the hypercapnic period if $\Delta S(t)$ did not show the expected decline at the end of hypercapnia. The analysis was conducted for ΔC_{HbO} and ΔC_{Hb} time courses derived from each of the three moments acquired at $r_{SD} = 1$ and 3 cm and for BF_i time courses acquired at $r_{SD} = 1$ and 2.7 cm.

2.6. Statistical analysis

All data are presented as mean \pm standard deviation unless otherwise noted. Statistical analyses were conducted using SPSS 16.0 (SPSS, Chicago, IL) and statistical significance was defined as $p < 0.05$. A two-way repeated-measures analysis of variance was used to investigate differences in each fitting parameter (τ , t_0 and ssCVR) for ΔC_{HbO} and ΔC_{Hb} derived from ΔN , $\Delta \langle t \rangle$, and ΔV ($r_{\text{SD}} = 3$ cm). The Student's t-test was used to investigate differences in each fitting parameter obtained from the analysis of the DCS data at $r_{\text{SD}} = 1$ and 2.7 cm.

Correlation analysis was performed to assess the depth sensitivity of DCS by investigating the agreement between the BF_i times course measured at $r_{\text{SD}} = 2.7$ cm and the corresponding ΔC_{HbO} and ΔC_{Hb} time courses derived from ΔN , $\Delta \langle t \rangle$, and ΔV ($r_{\text{SD}} = 3$ cm). This analysis was conducted for the period beginning with the start of hypercapnia to 1 min after hypercapnia. A second correlation was performed to investigate the relationship between the input P_{ETCO_2} waveform and the corresponding hemodynamic responses. For this analysis, the ΔC_{HbO} and ΔC_{Hb} time-courses derived from ΔN , $\Delta \langle t \rangle$, and ΔV ($r_{\text{SD}} = 3$ cm) were correlated to the corresponding time-varying changes in P_{ETCO_2} measured by the RespirAct. This analysis was also conducted for the ΔC_{HbO} and ΔC_{Hb} time-courses derived from the least-squares optimization approach.

3. Results

3.1. Crosstalk evaluation

The contamination of recorded DTOFs due to light emission from the DCS laser resulted in a slight rise in the background signal. The magnitude of this error averaged across the four participants and both wavelengths was $1.15 \pm 0.75\%$ at $r_{\text{SD}} = 1$ cm and $0.36 \pm 0.15\%$ at $r_{\text{SD}} = 3$ cm. Similarly, light from the two TR-NIRS lasers had only minor effects on the measured autocorrelation curves. Relative to autocorrelation curves acquired without signal contamination, the average difference in BF_i was $1.47 \pm 7.20\%$ at $r_{\text{SD}} = 1$ cm and $1.40 \pm 4.26\%$ at $r_{\text{SD}} = 2.7$ cm.

3.2. CVR experiments

Of the eleven participants, two were omitted from the data analysis. One due to poor skin-to-probe contact, resulting in poor signal to noise, and the other because the participant could not tolerate a P_{ETCO_2} increase of 15 mmHg. Of the remaining nine participants, the computer-controlled gas controller produced highly reproducible P_{ETCO_2} changes for all subjects. The average P_{ETCO_2} increase was 14.2 ± 0.6 mmHg, very close to the target of 15 mmHg with no significant differences found across the three intervals. Figure 1 presents the average time courses of changes in HR and MAP across subjects. For each participant, the data across the three hypercapnic challenges was combined into one 7-minute plot consisting of 2 minutes of hypercapnia, followed by a 5-min recovery period.

Figure 2 displays oxygenation and blood flow time courses from one subject. Every subplot includes the P_{ETCO_2} time course to illustrate its relationship to the measured responses. The top two rows display the ΔC_{HbO} and ΔC_{Hb} time series derived by moment analysis applied to the data collected at $r_{\text{SD}} = 3$ cm. The ΔC_{Hb} responses were inverted to help illustrate their temporal relationship to the P_{ETCO_2} time course. The bottom row presents the corresponding ΔC_{HbO} and negative ΔC_{Hb} time courses derived from the ΔN recorded at $r_{\text{SD}} = 1$ cm (as it has the greatest sensitivity to oxygenation changes in the scalp), along with the BF_i time courses from DCS data acquired at $r_{\text{SD}} = 1$ and 2.7 cm.

Figure 3 displays ΔC_{HbO} and ΔC_{Hb} time courses averaged across all nine subjects. Data are presented for both source-detector separations and each of the three moments. These time courses illustrate how the dynamics of the hypercapnic response varied with r_{SD} and statistical moment. The corresponding average ΔBF_i time courses from the two source-detectors separations are shown in the bottom row of Fig. 3. The figure (2nd row) also includes the brain ΔC_{HbO} and ΔC_{Hb}

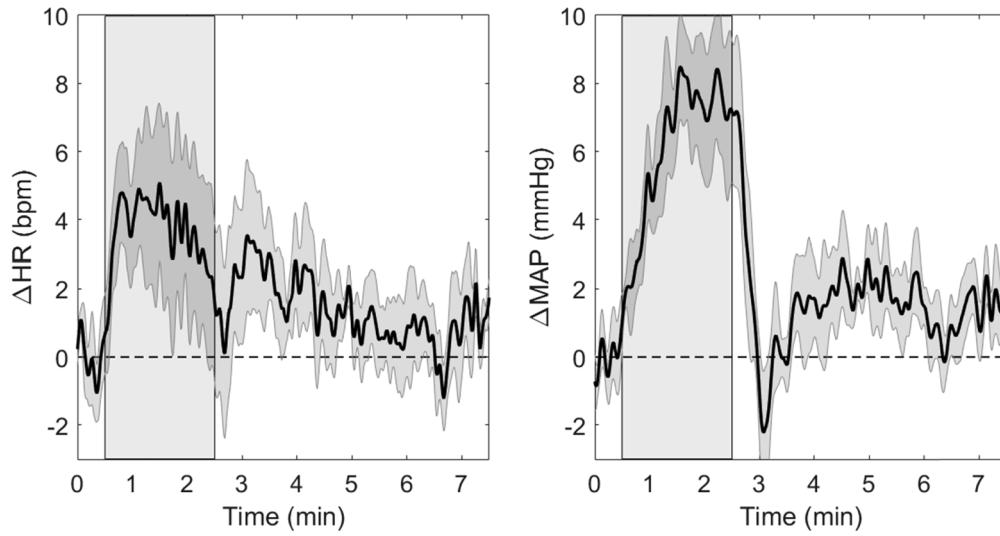


Fig. 1. Average change in heart rate (ΔHR) and mean arterial pressure (ΔMAP) across all subjects. Grey region represents the 2-min hypercapnic challenge and shading surrounding each line represents the standard error of the mean.

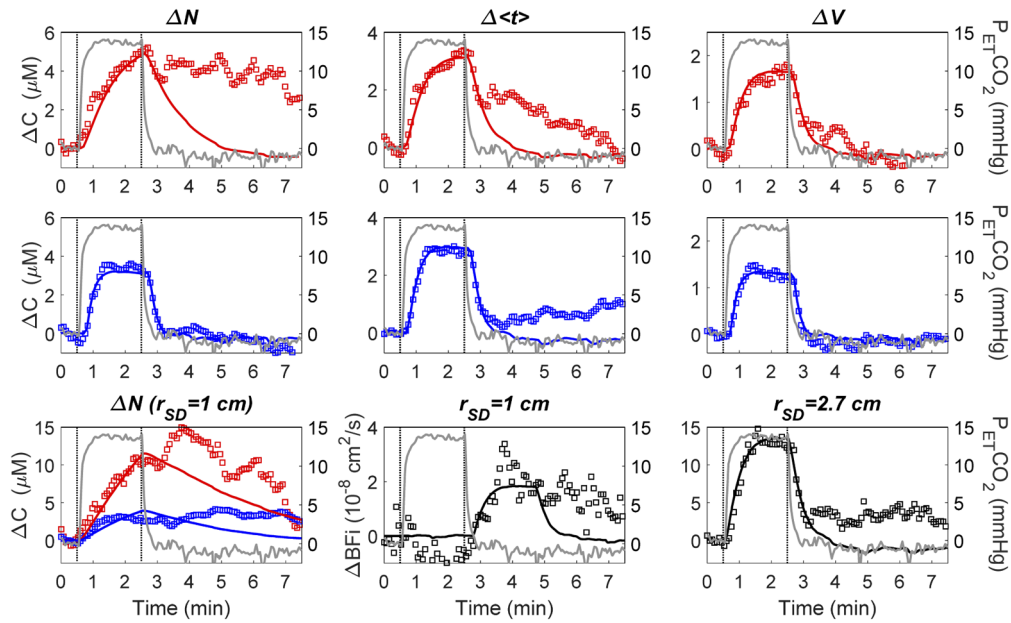


Fig. 2. TR-NIRS and DCS data from one participant. Top row displays ΔC_{HbO} (red squares) derived from moment analysis (ΔN , $\Delta\langle t \rangle$, ΔV) applied to DTOFs acquired at $r_{\text{SD}} = 3.0$ cm. Middle row displays the corresponding inverted ΔC_{Hb} (blue squares). Bottom row displays ΔC_{HbO} and inverted ΔC_{Hb} determined from ΔN at $r_{\text{SD}} = 1.0$ cm and ΔBF_i (black squares) time courses measured at $r_{\text{SD}} = 1.0$ and 2.7 cm. The best fit of the hemodynamic model is illustrated in each graph by the solid coloured line, and the grey line is the recorded ΔP_{ETCO_2} .

time courses derived from regressing ΔN measured at $r_{SD} = 1$ (ΔN_{1cm}) from ΔN measured at 3 cm (ΔN_{3cm}).

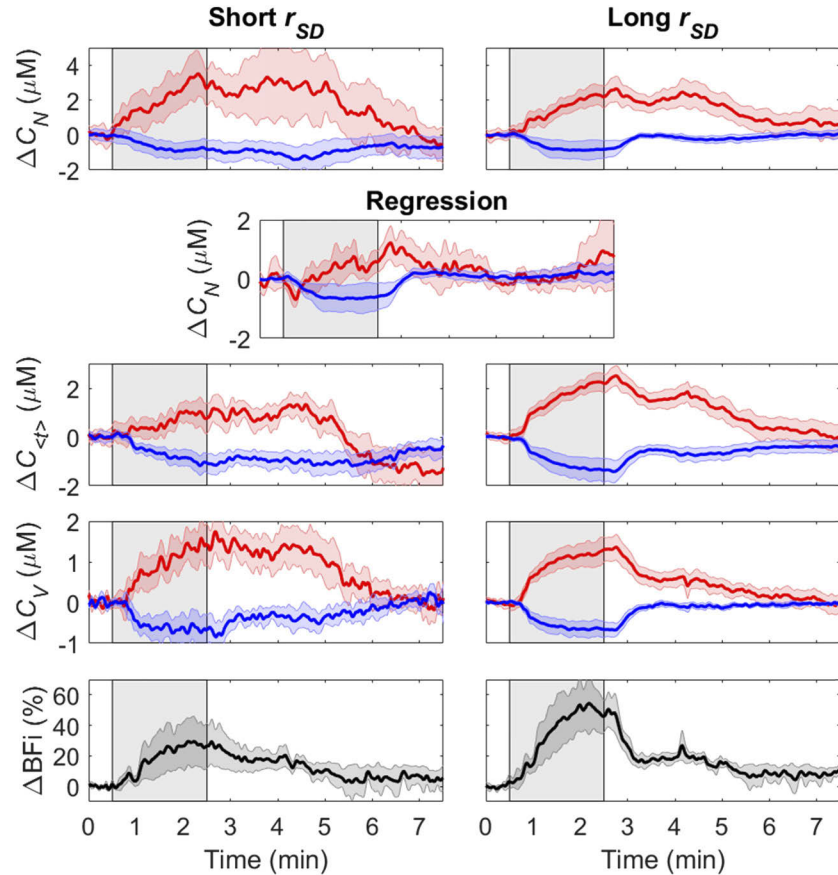


Fig. 3. Average ΔC_{HbO} , ΔC_{Hb} and ΔBF_i responses (red, blue and black, respectively) to the 2-min hypercapnic challenge (indicated by the shaded region). Time courses are presented for the two source-detector separations ($r_{SD} = 1$ and 3 cm for TR NIRS; $r_{SD} = 1$ and 2.7 cm for DCS). In addition, the second row provides the ΔC_{HbO} and ΔC_{Hb} responses determined by regressing ΔN_{1cm} from ΔN_{3cm} . All time courses were averaged across nine subjects. Shading surrounding each line represents the standard error of the mean.

The correlation coefficient relating the ΔBF_i hypercapnic response ($r_{SD} = 2.7$ cm) to the corresponding oxygenation responses ($r_{SD} = 3$ cm) was 0.24 ± 0.33 for ΔN , 0.80 ± 0.09 for $\Delta <t>$, and 0.72 ± 0.18 for ΔV . These values were averaged for ΔC_{HbO} and ΔC_{Hb} as there was no statistical difference between regression analyses for the two hemoglobin time courses. The correlation coefficient relating ΔBF_i to ΔN was significantly lower than the corresponding values relating ΔBF_i to $\Delta <t>$ and ΔV .

Correlating the P_{ETCO_2} time course to the corresponding ΔC_{HbO} time courses from the three moments ($r_{SD} = 3$ cm) resulted in coefficients of 0.09 ± 0.29 for ΔN , 0.29 ± 0.28 for $\Delta <t>$, and 0.49 ± 0.21 for ΔV . The corresponding coefficients for ΔC_{Hb} were 0.37 ± 0.51 (ΔN), 0.39 ± 0.31 ($\Delta <t>$) and 0.66 ± 0.20 (ΔV). This analysis was conducted for the entire 7 minutes to capture the observed differences in the residue signals for the three moments after the hypercapnic challenge (Fig. 3). For oxyhemoglobin, the correlation between P_{ETCO_2} and ΔN was significantly different from the correlation between P_{ETCO_2} and ΔV . There were no significant differences for the

correlation analysis involving the ΔC_{Hb} time courses. The correlation analysis was also conducted using the ΔC_{HbO} and ΔC_{Hb} time courses obtained from least-squares optimization; however, the coefficients (0.08 ± 0.31 for ΔC_{HbO} and 0.37 ± 0.57 for ΔC_{Hb}) did not improve relative to analyzing the ΔN_{3cm} separately.

Figure 4 presents box plots summarizing the fitting results for the ΔC_{HbO} and ΔC_{Hb} data recorded at $r_{SD} = 1$ cm (top row) and 3 cm (middle row), and BFi data recorded at $r_{SD} = 1$ and 2.7 cm (bottom row). For the data acquired at $r_{SD} = 3$ cm, ANOVA revealed a significant difference in ssCVR derived from ΔC_{HbO} and ΔC_{Hb} , as well as a lower ssCVR for ΔV compared to the other two moments. There were no significant differences in the analysis of the τ and t_0 data sets across the three moments or between BFi values from the two distances. This is explained by the high variability observed in parameters sensitive to scalp hemodynamics, such as BFi measured at $r_{SD} = 1$ cm, and ΔC_{HbO} derived from ΔN . For example, t_0 values for ΔN at $r_{SD} = 3$ cm ranged from 0 to 2 min – the latter is equivalent to the duration of hypercapnia – whereas the largest t_0 estimate for ΔV was 18 s. This variability was also reflected in the sum of squares when fitting Eq. (3) to the individual time courses. For example, at $r_{SD} = 3$ cm, the sum of squares for ΔC_{HbO} was 13.6 ± 15.2 for ΔN versus 8.0 ± 7.2 for ΔV . Likewise, the values for ΔC_{Hb} were 5.1 ± 12.4 and 0.9 ± 1.8 for ΔN and ΔV , respectively. Although the sum of squares decreased for the higher moments, this trend did not reach statistical significance.

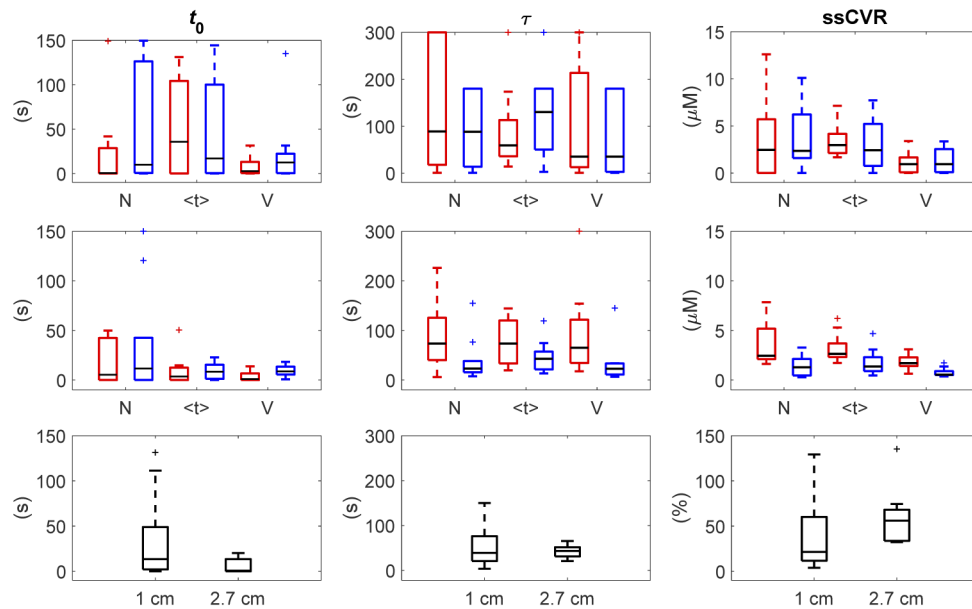


Fig. 4. Box plots of the three fitting parameters. From left to right: time delay (t_0), time constant (τ), and steady-state cerebrovascular reactivity (ssCVR). Results are presented for moment analysis applied to TR-NIRS data recorded at $r_{SD} = 1$ cm (top row), $r_{SD} = 3$ cm (middle row) and for DCS data acquired at the two r_{SD} values (bottom row). For the oxygenation results, red indicates ΔC_{HbO} and blue ΔC_{Hb} . Outliers are represented by the crosses, and in one case (τ for $\Delta C_{HbO,V}$), the outlier reached the upper fitting boundary of 250 s.

The average best-fit values of t_0 , τ and ssCVR from the analysis of ΔC_{HbO} , ΔC_{Hb} and BFi are provided in Table 1. The mean value for ΔC_{HbO} obtained from the variance does not include the outlier that reached the upper boundary of $\tau = 250$ s.

Figure 5 presents ΔCBF , ΔStO_2 and ΔCBV (i.e. ΔC_{tHb}) responses averaged across all subjects. Each response was scaled between 0 to 1 to demonstrate their temporal relationships. These time

Table 1. Best fit estimates of the time delay (t_0), time constant (τ), and steady-state cerebrovascular reactivity (ssCVR) obtained from the analysis of the ΔC_{HbO} , ΔC_{Hb} data derived from the three moments and BFi data derived for short and long r_{SD} . Values are presented as average (standard deviation).

| | t_0 (s) | | | τ (s) | | | ssCVR (μM) (% for BFi) | | |
|--------------------------|---------------|---------------------|---------------|---------------|---------------------|---------------|-------------------------------|---------------------|---------------|
| | N | $\langle t \rangle$ | V | N | $\langle t \rangle$ | V | N | $\langle t \rangle$ | V |
| HbO_{1cm} | 47 (45) | 26 (37) | 31 (40) | 124 (133) | 91 (91) | 120 (99) | 8.1 (10.5) | 3.5 (1.7) | 2.9 (1.3) |
| Hb_{1cm} | 55 (66) | 47 (60) | 25 (43) | 100 (81) | 113 (73) | 72 (83) | 4.0 (3.5) | 2.9 (2.7) | 2.8 (1.3) |
| HbO_{3cm} | 18 (22) | 10 (16) | 4 (5) | 87 (70) | 75 (45) | 73 (47) | 3.8 (2.2) | 3.2 (1.5) | 1.9 (0.7) |
| Hb_{3cm} | 22 (41) | 9 (8) | 9 (6) | 40 (48) | 46 (34) | 33 (43) | 1.4 (1.0) | 1.7 (1.4) | 0.8 (0.5) |
| | <i>1.0 cm</i> | | <i>2.7 cm</i> | <i>1.0 cm</i> | | <i>2.7 cm</i> | <i>1.0 cm</i> | | <i>2.7 cm</i> |
| BFi | 34 (51) | | 5.6 (7.8) | 52 (45) | | 42 (15) | 42 (45) | | 59 (33) |

courses were derived from measurements that provided the greatest depth sensitivity. That is, BFi measured at $r_{SD} = 2.7$ cm was chosen to represent CBF, and ΔC_{HbO} and ΔC_{Hb} derived from ΔV at $r_{SD} = 3$ cm were used to determine ΔStO_2 and ΔCBV . Mean increases were $7.6 \pm 3.6\%$ for ΔStO_2 and $0.52 \pm 0.81 \mu M$ for ΔC_{tHb} .

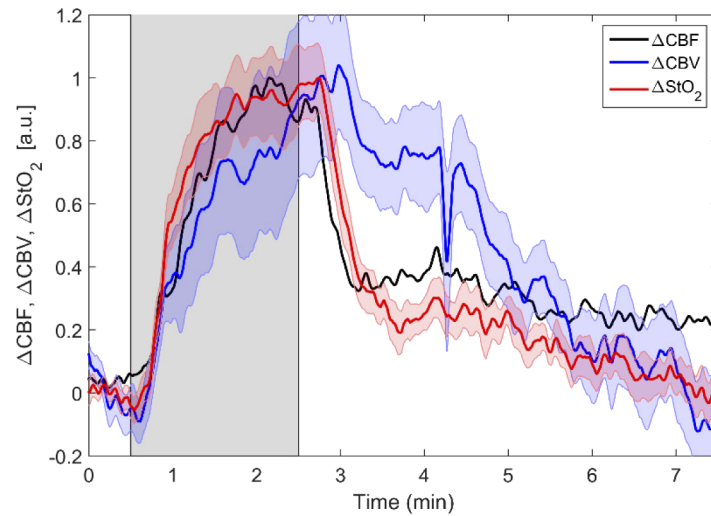


Fig. 5. Relative changes in cerebral blood flow (ΔCBF), cerebral blood volume (ΔCBV) and tissue oxygen saturation (ΔStO_2) during hypercapnia. Time courses were averaged across nine subjects. Shaded region represents hypercapnic period and the shading surrounding each line represents the standard error of the mean.

4. Discussion

This study presents the characterization of dynamic CVR in healthy adults by a hybrid TR-NIRS/DCS system. Simultaneous acquisition of blood flow and oxygenation data required minimizing crosstalk between the two devices. In initial tests on tissue-mimicking phantoms (data not presented), short-pass filters were found to be sufficient to eliminate contamination from the DCS laser on measured DTOFs. Similarly, the physical separation of the TR-NIRS pulsed lasers from the DCS detectors was sufficient to minimize any influence on recorded autocorrelation curves. This was confirmed by comparing BFi estimates from data acquired with and without the pulsed lasers running. The deviation in the BFi values under the two conditions

was less than 1% for data acquired at both $r_{SD} = 1$ and 2.7 cm. In vivo tests similarly showed small magnitudes of contaminations for both sets of measurements, although slightly higher variability between subjects, likely due to variations in probe-to-skin contact.

One of the main objectives of the study was to assess the impact of extra-cerebral signal contamination on TR NIRS and DCS, considering this is one of the major sources of error with these optical techniques. For this purpose, data from both devices were acquired at two source-detector separations with the short distance ($r_{SD} = 1$ cm) predominately reflecting scalp hemodynamics. For TR NIRS, moment analysis was also implemented to further enhance the separation of scalp and brain [36,37]. The mean time courses for the two source-detector separations and three moments demonstrated clear differences during hypercapnia and the recovery phase (Fig. 3). Most notably, the ΔC_{HbO} and ΔC_{Hb} responses derived from ΔV at $r_{SD} = 3$ cm were more similar to the expected CVR for a healthy brain (i.e., a rapid rise and fall in response to a step change in $P_{ET}CO_2$) [17,18]. In contrast, the responses for ΔN and $\Delta \langle t \rangle$ were distorted, as evident by the large residue signals observed after $P_{ET}CO_2$ had returned to normocapnia, particularly for ΔC_{HbO} . These observations reflect the differences in the correlation coefficients relating the oxygenation time courses to the $P_{ET}CO_2$ time course, which is driving the cerebrovascular response. The coefficient was only 0.09 ± 0.29 for ΔC_{HbO} derived from ΔN compared to 0.49 ± 0.21 when ΔC_{HbO} was derived from ΔV . These differences were also reflected by the residual when the hemodynamic model, Eq. (3), was fit to the oxygenation responses. The sum of squares was 13.6 ± 15.2 and 5.1 ± 12.4 for ΔC_{HbO} and ΔC_{Hb} derived from ΔN versus 8.0 ± 7.2 and 0.9 ± 1.8 for ΔC_{HbO} and ΔC_{Hb} derived from ΔV .

The time courses shown in Fig. 3 also illustrate that the consistency of the oxygenation response across the three moments was less for ΔC_{HbO} compared to ΔC_{Hb} . For ΔC_{HbO} , the correlation coefficient relating the response to $P_{ET}CO_2$ was roughly five times greater for ΔV compared to ΔN , while this ΔV -to- ΔN ratio was less than a factor of two for ΔC_{Hb} . This difference indicates that the deoxyhemoglobin signal was less sensitive to scalp hemodynamics and, consequently, a better measure of CVR. This finding is in contrast to a recent study that recommended using oxyhemoglobin to measure CVR [11]. However, greater sensitivity of deoxyhemoglobin to cerebral hemodynamics agrees with Kirilina et al. [38], who showed that changes in scalp blood flow caused by task-evoked sympathetic activity had a greater effect on oxyhemoglobin than deoxyhemoglobin. Extra-cerebral signal contamination also contributed to greater variability in CVR obtained from ΔC_{HbO} , as indicated by the coefficient of variation of ssCVR for ΔN_{3cm} , which was three times as large as the value for ΔV_{3cm} (Table 1). Scalp contributions to this variability is evident by the ΔC_{HbO} time course for ΔN_{1cm} , which showed the greatest fluctuations across subjects. This finding helps explain the inconsistency in CVR measurements reported in previous NIRS studies and highlights the importance of enhancing depth sensitivity [9,12].

Similar to the oxygenation results, DCS time courses acquired at the two source-detector distances exhibited different depth sensitivities (Fig. 3). The BF_i response at $r_{SD} = 2.7$ cm was larger and had a more pronounced decline at the end of hypercapnia, again in agreement with CVR expected in a healthy brain. The sensitivity of DCS to CBF is reflected by the difference in correlation of the BF_i response to the corresponding oxygenation responses derived from ΔN_{3cm} , $\Delta \langle t \rangle_{3cm}$ and ΔV_{3cm} . That is, the correlation to ΔN_{3cm} was significantly poorer than the correlation to the two higher moments. This is despite the fact that the DCS data were acquired with a continuous-wave laser, which does not provide the depth advantages of time-resolved detection [39]. The better correlation with higher moments can be understood by considering the DCS signal is directly proportional to blood flow, which is considerably higher in brain than scalp [9]. The mean CVR for the BF_i response measured at $r_{SD} = 2.7$ cm was $4.2 \pm 2.3\%$ per mmHg (defined as $ssCVR/\Delta P_{ET}CO_2$), which is good agreement with MRI-based perfusion studies that reported CVR values between 4 to 5% for similar increases in $P_{ET}CO_2$ [40–43].

The second main objective of the study was to evaluate if the speed of CVR in response to a rapid change in $P_{ET}CO_2$ could be characterized by a linear, time-invariant model with an exponential impulse response function. This approach was previously used to show slower vascular reactivity in patients with large artery steno-occlusive disease, indicating greater vascular resistance [17]. Focusing on metrics with the greatest depth sensitivity, average τ values were 42 ± 15 s for BF_i at $r_{SD} = 2.7$ cm, 33 ± 42 s for ΔC_{Hb} derived from ΔV_{3cm} , and 72 ± 51 s for the corresponding ΔC_{HbO} . These values were similar to those reported in BOLD studies of dynamic CVR: average grey-matter $\tau \sim 27$ s with a range from approximately 15 to 40 s [17,44,45]. Only τ for ΔC_{Hb} was within the MRI range, suggesting that these optical techniques could benefit from further improvement in separating oxygenation and flow responses in scalp and brain, such as using multilayered models [22,51,52]. However, implementing such models is more demanding as they typically require additional input parameters, in particular an estimate of the distance from the scalp to the brain.

The average τ values for the CBF and oxygenation responses were not significantly different, which is understandable considering MRI studies have shown that BOLD contrast, which predominately reflect ΔC_{Hb} , is a good surrogate of CBF for characterizing CVR [3]. However, altering basal vascular tone has been shown to affect BOLD-based CVR more than CBF-based CVR [46], and age-related CVR changes were larger for BOLD than CBF [47]. These findings reflect the fact that the relationship between blood oxygenation and blood flow is influenced by changes in arterial and venous blood volumes. Consequently, simultaneous monitoring of StO_2 and CBF (e.g. Fig. 5) may help detect disease or age-related changes in vascular function that would not be evident by measuring only one marker of CVR. This approach could be extended to incorporate an appropriate hemodynamic model to characterize underlying changes in cerebrovascular resistance [48,49].

A potential limitation with this study was that blood flow and oxygenation changes were only measured in response to a single increase in $P_{ET}CO_2$ of 15 mmHg. Given the ability of TR-NIRS/DCS to track rapid changes, it would be valuable to measure CBF and oxygenation responses to a series of step changes. Considering the $P_{ET}CO_2$ target in this study also evoked an increase in MAP (Fig. 1), measurements with smaller $P_{ET}CO_2$ changes would help elucidate if the relationship between CBF and oxygenation is altered by variations in the contributions from CO_2 reactivity and blood pressure [50].

5. Conclusion

This study presents the characterization of dynamic CBF and tissue oxygenation in response to a step increase in $P_{ET}CO_2$. Using a multi-distance TR-NIRS/DCS system enabled these hemodynamic responses to be measured simultaneously from the same brain region. The differences in the time courses from the two source-detector distances for both TR NIRS and DCS demonstrated that CO_2 vascular reactivity in scalp tissue was markedly slower than in brain. More importantly, scalp signal contamination resulted in significant distortions of CVR time courses across participants, particularly for ΔC_{HbO} . This contamination was substantially reduced by taking advantage of the greater depth sensitivity provided by TR NIRS. The time constant τ characterizing reactivity speed was found to be similar for CBF and tissue oxygenation in the healthy brain. Given the ease-of-use, portability, and non-invasiveness of this hybrid optical approach, it is well suited to investigate if the temporal relationship between CBF and oxygenation is altered by factors such as age, fitness level, and cerebrovascular disease.

Funding

Canadian Institutes of Health Research (130391); Natural Sciences and Engineering Research Council of Canada (R3592A02002).

Disclosures

The authors declare that they have no conflict of interest.

References

1. A. A. Phillips, F. H. Chan, M. M. Z. Zheng, A. V. Krassioukov, and P. N. Ainslie, "Neurovascular coupling in humans: Physiology, methodological advances and clinical implications," *J. Cereb. Blood Flow Metab.* **36**(4), 647–664 (2016).
2. J. J. Chen, "Cerebrovascular-Reactivity Mapping Using MRI: Considerations for Alzheimer's Disease," *Front. Aging Neurosci.* **10**, 170 (2018).
3. J. A. Fisher, L. Venkatraghavan, and D. J. Mikulis, "Magnetic Resonance Imaging–Based Cerebrovascular Reactivity and Hemodynamic Reserve," *Stroke* **49**(8), 2011–2018 (2018).
4. M. J. Donahue, L. M. Dethrage, C. C. Faraco, L. C. Jordan, P. Clemmons, R. Singer, J. Mocco, Y. Shyr, A. Desai, A. O'Duffy, D. Riebau, L. Hermann, J. Connors, H. Kirshner, and M. K. Strother, "Routine Clinical Evaluation of Cerebrovascular Reserve Capacity Using Carbogen in Patients With Intracranial Stenosis," *Stroke* **45**(8), 2335–2341 (2014).
5. C. K. Willie, F. L. Colino, D. M. Bailey, Y. C. Tzeng, G. Binsted, L. W. Jones, M. J. Haykowsky, J. Bellapart, S. Ogoh, K. J. Smith, J. D. Smirl, T. A. Day, S. J. Lucas, L. K. Eller, and P. N. Ainslie, "Utility of transcranial Doppler ultrasound for the integrative assessment of cerebrovascular function," *J. Neurosci. Methods* **196**(2), 221–237 (2011).
6. N. S. Coverdale, J. S. Gati, O. Opalevych, A. Perrotta, and J. K. Shoemaker, "Cerebral blood flow velocity underestimates cerebral blood flow during modest hypercapnia and hypocapnia," *J. Appl. Physiol.* **117**(10), 1090–1096 (2014).
7. P. Smielewski, P. Kirkpatrick, P. Minhas, J. D. Pickard, and M. Czosnyka, "Can Cerebrovascular Reactivity Be Measured With Near-Infrared Spectroscopy?" *Stroke* **26**(12), 2285–2292 (1995).
8. T. Alderliesten, P. M. A. Lemmers, J. J. M. Smarius, R. E. van de Vosse, W. Baerts, and F. van Bel, "Cerebral oxygenation, extraction, and autoregulation in very preterm infants who develop peri-intraventricular hemorrhage," *J. Pediatr.* **162**(4), 698–704.e2 (2013).
9. J. Selb, D. A. Boas, S.-T. Chan, K. C. Evans, E. M. Buckley, and S. A. Carp, "Sensitivity of near-infrared spectroscopy and diffuse correlation spectroscopy to brain hemodynamics: simulations and experimental findings during hypercapnia," *Neurophotonics* **1**(1), 015005 (2014).
10. T. S. Leung, I. Tachtsidis, M. M. Tisdall, C. Pritchard, M. Smith, and C. E. Elwell, "Estimating a modified Grubb's exponent in healthy human brains with near infrared spectroscopy and transcranial Doppler," *Physiol. Meas.* **30**(1), 1–12 (2009).
11. F. Amyot, K. Kenney, E. Spessert, C. Moore, M. Haber, E. Silverman, A. Gandjbakhche, and R. Diaz-Arrastia, "Assessment of cerebrovascular dysfunction after traumatic brain injury with fMRI and fNIRS," *NeuroImage Clin.* **25**(102086), 102086 (2020).
12. J. Virtanen, T. Noponen, and P. Meriläinen, "Comparison of principal and independent component analysis in removing extracerebral interference from near-infrared spectroscopy signals," *J. Biomed. Opt.* **14**(5), 054032 (2009).
13. W. A. C. Mutch, S. R. Patel, A. M. Shahidi, S. I. Kulasekara, J. A. Fisher, J. Duffin, and C. Hudson, "Cerebral Oxygen Saturation: Graded Response to Carbon Dioxide with Isoxia and Graded Response to Oxygen with Isocapnia," *PLoS One* **8**(2), e57881 (2013).
14. T. Durduran, R. Choe, W. B. Baker, and A. G. Yodh, "Diffuse optics for tissue monitoring and tomography," *Rep. Prog. Phys.* **73**(7), 076701 (2010).
15. L. He, W. B. Baker, D. Milej, V. C. Kavuri, R. C. Mesquita, D. R. Busch, K. Abramson, Y. J. Jiang, M. Diop, K. St. Lawrence, O. Amendolia, F. Quattrone, R. Balu, W. A. Kofke, and A. G. Yodh, "Noninvasive continuous optical monitoring of absolute cerebral blood flow in critically ill adults," *Neurophotonics* **5**(4), 045006 (2018).
16. M. J. Poulin, P. J. Liang, and P. A. Robbins, "Dynamics of the cerebral blood flow response to step changes in end-tidal PCO₂ and PO₂ in humans," *J. Appl. Physiol.* **81**(3), 1084–1095 (1996).
17. J. Poubanc, A. P. Crawley, O. Sobczyk, G. Montandon, K. Sam, D. M. Mandell, P. Dufort, L. Venkatraghavan, J. Duffin, D. J. Mikulis, and J. A. Fisher, "Measuring cerebrovascular reactivity: the dynamic response to a step hypercapnic stimulus," *J. Cereb. Blood Flow Metab.* **35**(11), 1746–1756 (2015).
18. J. Duffin, O. Sobczyk, A. P. Crawley, J. Poubanc, D. J. Mikulis, and J. A. Fisher, "The dynamics of cerebrovascular reactivity shown with transfer function analysis," *NeuroImage* **114**, 207–216 (2015).
19. M. Slessarev, J. Han, A. Mardimae, E. Prisman, D. Preiss, G. Volgyesi, C. Ansel, J. Duffin, and J. A. Fisher, "Prospective targeting and control of end-tidal CO₂ and O₂ concentrations," *J. Physiol.* **581**(3), 1207–1219 (2007).
20. A. Torricelli, D. Contini, A. Pifferi, M. Caffini, R. Re, L. Zucchelli, and L. Spinelli, "Time domain functional NIRS imaging for human brain mapping," *NeuroImage* **85**(1), 28–50 (2014).
21. A. Abdalmalak, D. Milej, M. Diop, M. Shokouhi, L. Naci, A. M. Owen, and K. St. Lawrence, "Can time-resolved NIRS provide the sensitivity to detect brain activity during motor imagery consistently?" *Biomed. Opt. Express* **8**(4), 2162 (2017).
22. D. Milej, L. He, A. Abdalmalak, W. B. Baker, U. C. Anazodo, M. Diop, S. Dolui, V. C. Kavuri, W. Pavlosky, L. Wang, R. Balu, J. A. Detre, O. Amendolia, F. Quattrone, W. A. Kofke, A. G. Yodh, and K. St. Lawrence, "Quantification of cerebral blood flow in adults by contrast-enhanced near-infrared spectroscopy: Validation against MRI," *J. Cereb. Blood Flow Metab.* 0271678X1987256 (2019).

23. A. Abdalmalak, D. Milej, L. Norton, D. B. DeBicki, T. Gofton, M. Diop, A. M. Owen, and K. St. Lawrence, "Single-session communication with a locked-in patient by functional near-infrared spectroscopy," *Neurophotonics* **4**(04), 1 (2017).
24. D. Milej, A. Abdalmalak, P. McLachlan, M. Diop, A. Liebert, K. St. Lawrence, and K. St. Lawrence, "Subtraction-based approach for enhancing the depth sensitivity of time-resolved NIRS," *Biomed. Opt. Express* **7**(11), 4514 (2016).
25. M. Kewin, A. Rajaram, D. Milej, A. Abdalmalak, L. Morrison, M. Diop, and K. St. Lawrence, "Evaluation of hyperspectral NIRS for quantitative measurements of tissue oxygen saturation by comparison to time-resolved NIRS," *Biomed. Opt. Express* **10**(9), 4789 (2019).
26. A. Abdalmalak, D. Milej, L. C. M. Yip, A. R. Khan, M. Diop, A. M. Owen, and K. St. Lawrence, "Assessing Time-Resolved fNIRS for Brain-Computer Interface Applications of Mental Communication," *Front. Neurosci.* **14**, 105 (2020).
27. D. Milej, A. Abdalmalak, D. Janusek, M. Diop, A. Liebert, and K. St. Lawrence, "Time-resolved subtraction method for measuring optical properties of turbid media," *Appl. Opt.* **55**(7), 1507 (2016).
28. M. Khalid, D. Milej, A. Rajaram, A. Abdalmalak, L. Morrison, M. Diop, and K. St. Lawrence, "Development of a stand-alone DCS system for monitoring absolute cerebral blood flow," *Biomed. Opt. Express* **10**(9), 4607 (2019).
29. M. Diop, K. M. Tichauer, J. T. Elliott, M. Migueis, T.-Y. Lee, and K. St. Lawrence, "Comparison of time-resolved and continuous-wave near-infrared techniques for measuring cerebral blood flow in piglets," *J. Biomed. Opt.* **15**(5), 057004 (2010).
30. A. Liebert, H. Wabnitz, D. Grosenick, M. Möller, R. Macdonald, H. Rinneberg, M. Moller, R. Macdonald, H. Rinneberg, M. Möller, R. Macdonald, and H. Rinneberg, "Evaluation of optical properties of highly scattering media by moments of distributions of times of flight of photons," *Appl. Opt.* **42**(28), 5785–5792 (2003).
31. D. Milej, D. Janusek, A. Gerega, S. Wojtkiewicz, P. Sawosz, J. Treszczanowicz, W. Weigl, and A. Liebert, "Optimization of the method for assessment of brain perfusion in humans using contrast-enhanced reflectometry: multidistance time-resolved measurements," *J. Biomed. Opt.* **20**(10), 106013 (2015).
32. M. Kacprzak, A. Liebert, P. Sawosz, N. Żolek, and R. Maniewski, "Time-resolved optical imager for assessment of cerebral oxygenation," *J. Biomed. Opt.* **12**(3), 034019 (2007).
33. R. B. Saager and A. J. Berger, "Direct characterization and removal of interfering absorption trends in two-layer turbid media," *J. Opt. Soc. Am. A* **22**(9), 1874–1882 (2005).
34. T. Durduran and A. G. Yodh, "Diffuse correlation spectroscopy for non-invasive, micro-vascular cerebral blood flow measurement," *NeuroImage* **85**(1), 51–63 (2014).
35. K. Verdecchia, M. Diop, L. B. Morrison, T.-Y. Lee, and K. St. Lawrence, "Assessment of the best flow model to characterize diffuse correlation spectroscopy data acquired directly on the brain," *Biomed. Opt. Express* **6**(11), 4288 (2015).
36. W. Weigl, D. Milej, A. Gerega, B. Toczyłowska, P. Sawosz, M. Kacprzak, D. Janusek, S. Wojtkiewicz, R. Maniewski, and A. Liebert, "Confirmation of brain death using optical methods based on tracking of an optical contrast agent: assessment of diagnostic feasibility," *Sci. Rep.* **8**(1), 7332 (2018).
37. D. Milej, A. Gerega, M. Kacprzak, P. Sawosz, W. Weigl, R. Maniewski, and A. Liebert, "Time-resolved multi-channel optical system for assessment of brain oxygenation and perfusion by monitoring of diffuse reflectance and fluorescence," *Opto-Electronics Rev.* **22**(1), 55–67 (2014).
38. E. Kirilina, A. Jelzow, A. Heine, M. Niessing, H. Wabnitz, R. Brühl, B. Itermann, A. M. Jacobs, and I. Tachtsidis, "The physiological origin of task-evoked systemic artefacts in functional near infrared spectroscopy," *NeuroImage* **61**(1), 70–81 (2012).
39. J. Sutin, B. Zimmerman, D. Tyulmankov, D. Tamborini, K. C. Wu, J. Selb, A. Gulinatti, I. Rech, A. Tosi, D. A. Boas, and M. A. Franceschini, "Time-domain diffuse correlation spectroscopy," *Optica* **3**(9), 1006–1013 (2016).
40. B. Dubois, H. H. Feldman, C. Jacova, J. L. Cummings, S. T. Dekosky, P. Barberger-Gateau, A. Delacourte, G. Frisoni, N. C. Fox, D. Galasko, S. Gauthier, H. Hampel, G. A. Jicha, K. Meguro, J. O'Brien, F. Pasquier, P. Robert, M. Rossor, S. Salloway, M. Sarazin, L. C. de Souza, Y. Stern, P. J. Visser, and P. Scheltens, "Revising the definition of Alzheimer's disease: a new lexicon," *Lancet Neurol.* **9**(11), 1118 (2010).
41. F. B. Tancredi and R. D. Hoge, "Comparison of Cerebral Vascular Reactivity Measures Obtained Using Breath-Holding and CO₂ Inhalation," *J. Cereb. Blood Flow Metab.* **33**(7), 1066–1074 (2013).
42. K. S. St. Lawrence, F. Q. Ye, B. K. Lewis, D. R. Weinberger, J. A. Frank, and A. C. McLaughlin, "Effects of indomethacin on cerebral blood flow at rest and during hypercapnia: an arterial spin tagging study in humans," *J. Magn. Reson. Imaging* **15**(6), 628–635 (2002).
43. U. C. Anazodo, J. K. Shoemaker, N. Suskin, T. Ssali, D. J. J. Wang, and K. S. St. Lawrence, "Impaired Cerebrovascular Function in Coronary Artery Disease Patients and Recovery Following Cardiac Rehabilitation," *Front. Aging Neurosci.* **7**, 224 (2016).
44. L. McKetton, O. Sobczyk, J. Duffin, J. Poublanc, K. Sam, A. P. Crawley, L. Venkatraghavan, J. A. Fisher, and D. J. Mikulis, "The aging brain and cerebrovascular reactivity," *NeuroImage* **181**, 132–141 (2018).
45. K. Sam, J. Conklin, K. R. Holmes, O. Sobczyk, J. Poublanc, A. P. Crawley, D. M. Mandell, L. Venkatraghavan, J. Duffin, J. A. Fisher, S. E. Black, and D. J. Mikulis, "Impaired dynamic cerebrovascular response to hypercapnia predicts development of white matter hyperintensities," *NeuroImage Clin.* **11**, 796–801 (2016).

46. S. Halani, J. B. Kwint, A. M. Golestani, Y. B. Khatamian, and J. J. Chen, "Comparing cerebrovascular reactivity measured using BOLD and cerebral blood flow MRI: The effect of basal vascular tension on vasodilatory and vasoconstrictive reactivity," *NeuroImage* **110**, 110–123 (2015).
47. C. J. Gauthier, C. Madjar, L. Desjardins-Crépeau, P. Bellec, L. Bherer, and R. D. Hoge, "Age dependence of hemodynamic response characteristics in human functional magnetic resonance imaging," *Neurobiol. Aging* **34**(5), 1469–1485 (2013).
48. J. M. Kainerstorfer, A. Sassaroli, K. T. Tgavalekos, and S. Fantini, "Cerebral Autoregulation in the Microvasculature Measured with Near-Infrared Spectroscopy," *J. Cereb. Blood Flow Metab.* **35**(6), 959–966 (2015).
49. S. J. Payne, J. Selb, and D. A. Boas, "Effects of autoregulation and CO₂ reactivity on cerebral oxygen transport," *Ann. Biomed. Eng.* (2009).
50. A. Battisti-Charbonney, J. Fisher, and J. Duffin, "The cerebrovascular response to carbon dioxide in humans," *J. Physiol.* **589**(12), 3039–3048 (2011).
51. K. Verdecchia, M. Diop, A. Lee, L. B. Morrison, T.-Y. Lee, and K. St. Lawrence, "Assessment of a multi-layered diffuse correlation spectroscopy method for monitoring cerebral blood flow in adults," *Biomed. Opt. Express* **7**(9), 3659 (2016).
52. W. B. Baker, A. B. Parthasarathy, T. S. Ko, D. R. Busch, K. Abramson, S.-Y. Tzeng, R. C. Mesquita, T. Durduran, J. H. Greenberg, D. K. Kung, and A. G. Yodh, "Pressure modulation algorithm to separate cerebral hemodynamic signals from extracerebral artifacts," *Neurophotonics* **2**(3), 035004 (2015).